GEOPHYSICS, VOL. 61, NO. 6 (NOVEMBER-DECEMBER 1996); P. 1689–1701, 10 FIGS., 2 TABLES.

Thermal analysis of the southern Powder River Basin, Wyoming

Brian J. O. L. McPherson* and David S. Chapman‡

ABSTRACT

Temperature and geologic data from over 3000 oil and gas wells within a 180 km × 30 km area that transect across the southern Powder River Basin in Wyoming, U.S.A., were used to determine the present thermal regime of the basin. Three-dimensional temperature fields within the transect, based on corrected bottom-hole temperatures (BHTs) and other geologic information, were assessed using: (1) A laterally constant temperature gradient model in conjunction with an L_1 norm inversion method, and (2) a laterally variable temperature gradient model in conjunction with a stochastic inversion technique. The mean geothermal gradient in the transect is 29°C/km, but important lateral variations in the geothermal gradient exist. The average heat flow for the southern Powder River Basin is 52 mW/m^2 with systematic variations between 40 mW/m^2 and 60 mW/m^2 along the transect. Extremely high local heat flow (values up to 225 mW/m^2) in the vicinity of the Teapot Dome and the Salt Creek Anticline and low heat flow of 25 mW/m^2 occurring locally near the northeast end of the transect are likely caused by groundwater movement.

INTRODUCTION

An accurate assessment of the present-day thermal state of a sedimentary basin, including temperature and heat-flow distributions, is helpful in resolving many basin-scale and intrabasin-scale processes. Hydrocarbon maturation, fluid migration, and diagenetic reactions all depend critically on temperature.

Evaluation of basin-scale temperature fields, however, is hampered by the lack of high-quality data. The primary temperature information available in sedimentary basins is obtained from bottom-hole temperatures (BHTs), temperatures measured at the bottom of oil and gas wells during geophysical logging. BHTs are systematically cooler than true formation temperatures because of disturbances associated with drilling; full temperature equilibration takes weeks whereas BHTs are typically measured within hours of drilling. They can also be contaminated by indeterminate measurement noise (Luheshi, 1983; Cao et al., 1988; and Deming, 1989). Measurement error and other noise necessitate statistical methods to extract the thermal signal and assess confidence levels.

Two models (Speece et al., 1985; Willett and Chapman, 1987a, 1987b) in conjunction with inversion techniques (Deming and Chapman, 1988b; Willett, 1990) developed to resolve spatial variation do appear to mitigate the effects of BHT data noise. However, because of the lack of available high-resolution temperature data, it is unclear which model best estimates actual temperature fields. A comparison of temperature fields and heat flow estimated using both models with a large, common data base seems to be warranted.

This study is an evaluation of the present-day thermal state, including temperature and heat-flow distributions, of part of the Powder River Basin, Wyoming. Several thousand wells were drilled for oil and gas exploration in this basin, providing a rich source of BHT information and the opportunity to compare the different methods of temperature analysis. Over 3000 well information cards were collected from which 1807 BHTs were used. The temperature models presented in Speece et al. (1985) and Willett and Chapman (1987a) were used with the inversion methods of Deming and Chapman (1988b) and Willett (1990) to construct the present-day temperature field. The results of the different models were compared to each other and a preferred temperature field, in conjunction with measured thermal conductivities and other geologic data, was used to estimate heat flow for the region.

THE POWDER RIVER BASIN

Geologic setting

The Powder River Basin is a large (30 000 km^2), intermontane synclinal basin located in northeastern Wyoming and

Manuscript received by the Editor January 21, 1993; revised manuscript received July 10, 1995.
*Formerly University of Utah, Department of Geology and Geophysics, Salt Lake City, UT 84112; presently New Mexico Tech, Department of Earth & Environmental Science, Socorro, New Mexico 87801.
‡University of Utah, Department of Geology and Geophysics, Salt Lake City, UT 84112.

southeastern Montana (Figure 1). The asymmetrical syncline has a north-south trending axis which is displaced west of the center of the basin. Structural highlands almost completely surround the basin: the Black Hills on the east, the Bighorn Mountains juxtaposed on the west, and the Hartville uplift and the Laramie Mountains on the south. The Yellowstone River forms the northern boundary in Montana. Flat rolling grasslands and broad valleys with high terraces and badlands surround the Powder, Cheyenne, Belle Fourche, and North Platte River systems. Average surface elevation of the basin is 1500 m. The southwestern side of the basin is generally 300 to 500 m higher in elevation than the northeastern side, reflecting the general drainage. Elevation in the area varies from 4015 m at Cloud Peak (Bighorn Mountains) to about 1100 m for the Powder River itself. Precambrian strata are found in the deepest part of the basin axis at 3600 m below sea level and crop out at 4000 m above sea level at Cloud Peak, implying a maximum structural relief of 7600 m. Most topographic features of the basin are a result of differences in erosional characteristics of Tertiary rocks and stream erosion (Sharp and Gibbons, 1964).

Structure and stratigraphy

The Powder River Basin is the deepest and one of the most extensive of a line of basins extending from central New Mexico to central Montana along the front of the Rocky Mountains. A generalized southwest-northeast cross-section through the Powder River Basin is shown in Figure 2. Formation tops from 2411 wells were used to construct the cross-section with additional constraint placed by the surface geology mapped by Love and Christiansen (1985). The asymmetric structure of profile A–A′ is uniform throughout the basin, with the steeper dipping beds west of the syncline axis. Regional dip on the eastern limb of the basin syncline is 2 degrees whereas dips up to 8 degrees occur on the western limb. According to Love and Christiansen (1985), no large-scale faults intersect the surface in the basin, nor are any subsurface faults evident.

A generalized stratigraphic column for the Powder River Basin is shown in Figure 3. Twenty-two primary formations from the Minnelusa formation (Pennsylvanian) up to the Wasatch formation (Eocene) at the surface are included. To

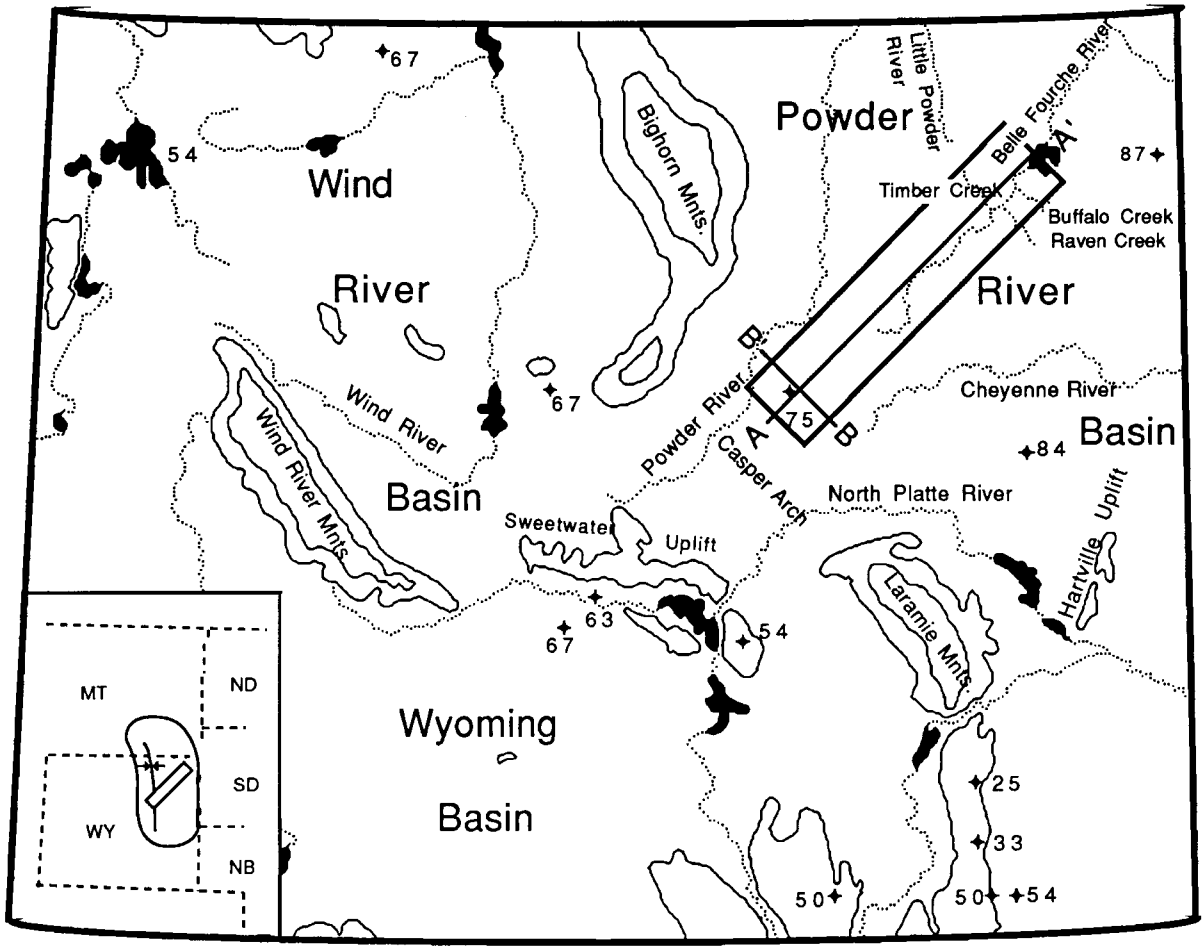

FIG. 1. Location map for the Powder River Basin. Inset shows basin location in the western U.S., the basin outline and axis, and the location of profile A–A′. Rivers are indicated by dotted lines, topographic contours are solid lines, and solid black patches indicate lakes. The geologic section along A–A′ is provided in Figure 2. Bold rectangle indicates detailed study region. Heat flow sites (crosses) and values in mW/m^2 from Blackwell (1969), Sass et al. (1971), and Decker et al. (1980).

facilitate and simplify the thermal analysis, these 22 formations were grouped into seven "lithothermal units" based on similarities in lithology and thermal properties. The Wasatch formation, the Ft. Union formation, and the Lance formation comprise lithothermal unit 1 (Figure 3); it is referred to as the Wasatch-Lance unit. Similarly, lithothermal units 2 through 7 are respectively referred to as the Fox Hills unit, the Pierre-Steele unit, the Niobrara-Belle Fourche unit, the Mowry-Dakota unit, the Spearfish-Chugwater unit, and the Minnelusa-Tensleep unit. The breakdown of lithothermal units is illustrated on Figure 3.

THERMAL DATA

Temperatures

Subsurface temperature information in sedimentary basins comes from BHTs, drill stem tests in oil and gas wells, and high-resolution temperature logs in holes drilled for mineral or water exploration. Mineral exploration boreholes are scarce in most basins and if available are usually shallow (depth less than 500 m). Temperature measurements in shallow wells must be corrected for topography, climate variations, and possible advective effects caused by shallow groundwater systems (Jaegar, 1965; Bauer and Chapman, 1986; Powell et al., 1988). Bottom-hole temperatures measured during geophysical logging of oil and gas wells to depths of several kilometers serve as an alternative data base.

Several thousand wells have been drilled in the Powder River Basin as a result of intense oil and gas exploration. Within the southern half of the basin, a transect (Figure 1) roughly perpendicular to the basin axis was selected for detailed study. Location of the transect on the groundwater drainage divide between the Powder and Cheyenne rivers should minimize advective effects of groundwater and surface drainage. The transect was also positioned to capture a high density of exploration wells and oil and gas fields. BHT measurement information and other geologic data for 3065 wells were read from geophysical well-log headers available at the Wyoming Oil and Gas Commission. Of these, 1807 had sufficient information for the thermal analysis. Well logs with insufficient temperature or measurement time information were discarded. Locations of wells used in this analysis are shown in Figure 4.

The BHT data were not used in raw form. In addition to operator error, recording error, and uncertain thermometer calibration, temperatures are measured immediately following mud circulation and the well is rarely given enough time to reach thermal equilibrium before measurement. Consequently, BHTs recorded on log headers are usually significantly lower than the undisturbed formation temperature and must be corrected (Bullard, 1947; Lee, 1982; Luheshi, 1983; Jones et al., 1984; Beck and Shen, 1985; Cao et al., 1988; Deming, 1989).

Depending on the amount of information provided in the drilling history, the BHTs used in this study received one of two different types of temperature correction. If a sequence of two or more temperature measurements at a single depth was available, a relaxation correction (Bullard, 1947; Horner, 1951) was applied. The equilibrium temperature is found from the sequence of temperatures $T(t)$ measured at time t after well shut in by

$$T(t) = T_\infty + A \ln\{(t + t_{\text{circ}})/t\}, \quad (1)$$

where t_{circ} is mud circulation time after reaching the logging depth and A is the slope of the relaxation plot. If only a single BHT and its time of measurement were recorded, a modified version of the depth-time correction used by Willett and Chapman (1987b) and Deming and Chapman (1988b) was applied. The relaxation curve slope is expressed as a quadratic function of depth, allowing for calibration in each basin being studied. For the Powder River Basin, our depth-time correction ΔT is

$$\Delta T = T_\infty - T(t) = -[az + bz^2]\ln[(t + t_{\text{circ}})/t], \quad (2)$$

where the coefficients are $a = -1.1 \times 10^{-2}$°C/m and $b = 1.8 \times 10^{-6}$°C/m^2. For this study, Horner plot corrections were applied to 198 of the 1807 wells, and depth-time corrections were applied to the remaining BHTs; corrections applied to this data set ranged from 1°C to 25°C. An uncertainty was estimated

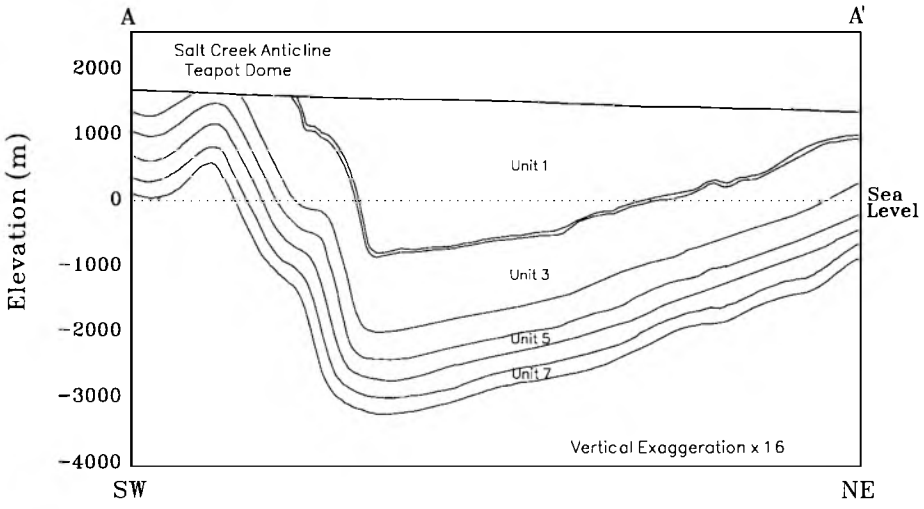

FIG. 2. Generalized cross-section for Powder River Basin study area. Location of profile A–A′ is shown on Figure 1. Units 1 through 7 denote lithothermal units used in the thermal analysis.

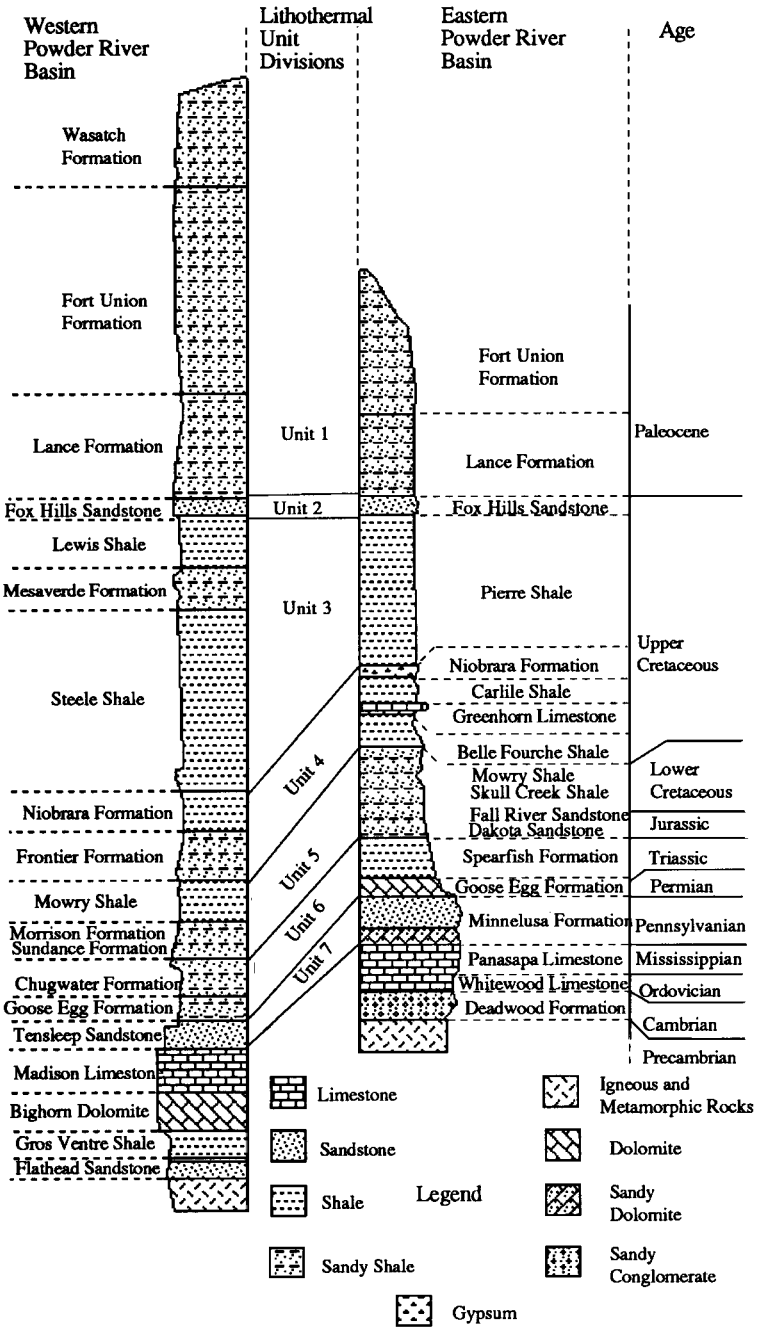

FIG. 3. Generalized stratigraphic column for the Powder River Basin. Adapted from Tenney (1966).

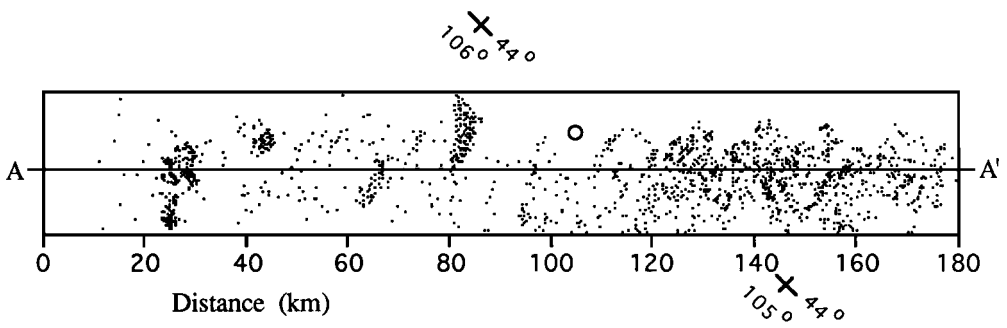

FIG. 4. Transect across the Powder River Basin showing the locations of oil and gas wells used in thermal analysis. The transect is 180 km long and 30 km wide. The open circle represents the location of the Government Davis no. 5 well used for detailed thermal conductivity measurements.

for each corrected temperature and varied from 2°C to 14°C. Details of both the Horner plot correction and the depth-time correction along with associated statistics are provided in McPherson (1992).

A composite plot of corrected BHTs versus depth for the 1807 wells in the southern Powder River Basin transect is shown in Figure 5. Linear least-squares regression of these data yields a mean geothermal gradient of 29°C/km. However, shallow wells display temperature gradients three to four times greater than this average. Temperatures increase with depth, but with considerable scatter; a typical variation of temperature for any given depth is about 35°C. This scatter must be attributed at least partially to geologically T_∞ caused spatial variations of the temperature field (Willett and Chapman, 1987a) because the standard error in corrected BHTs is generally less than 15°C. Although previous workers (Carvalho and Vacquier, 1977; Majorowicz and Jessop, 1981) have used average gradient models to evaluate temperatures and heat flow on a regional scale, these average gradient analyses do not permit resolution of lateral or vertical temperature variation. Methods of temperature analysis that are capable of resolving spatial variation were used for this study because of the large size of the Powder River Basin and the noise in the BHT data.

To determine local thermal gradients and heat flow, it is necessary to estimate surface ground temperature (SGT) at each well site. Although SGTs are seldom monitored, they can be deduced from surface air temperatures (SATs) published with other meteorologic data (National Oceanic and Atmospheric Administration, 1989). Twenty-five meteorologic stations throughout the region (Figure 1) were used to determine a linear least-squares estimating function for SATs based on latitude and elevation (McPherson, 1992):

$$\mathrm{SAT} = 9.7 - 0.0021h - 0.0042y \qquad (^\circ\mathrm{C}), \qquad (3)$$

where h is elevation in meters, and y is northing in kilometers from the southwest corner of the transect. Equation (3) was applied to the elevation and northing of each well site to estimate SATs within the transect.

Surface air temperatures are typically measured between 1 and 2 m above the ground surface and, especially in regions of winter snow cover, the mean annual air temperature is significantly lower than the mean annual ground temperature (see Figure 5.5 of Powell et al., 1988). Four meteorologic stations within our study area reported both SGTs and SATs; the mean annual SGT at these four stations is on average 3.2°C higher than the mean annual SAT. This value was added to SATs calculated by equation (3) to predict SGTs at all well sites throughout the basin transect.

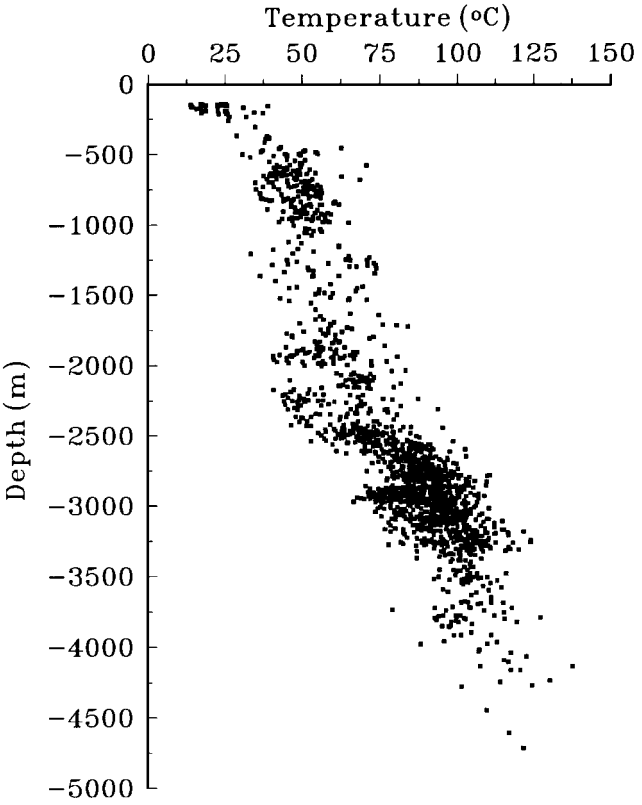

FIG. 5. Corrected BHTs versus depth for Powder River Basin transect. Surface ground temperatures along transect are close to 10°C.

Lithothermal unit thickness

The thermal analysis performed in this study also requires thickness for each lithothermal unit at every well site. This information could be assembled if each formation were identified in every well, or if structure maps for those formations bounding the lithothermal units were available. Unfortunately, the necessary maps are not available in the published literature.

Information recorded on well information cards often focuses on an exploration play and is incomplete for the remainder of the vertical section; thus, formation top information for any particular formation throughout the basin may be sparse or incomplete. Therefore, structure maps of the seven lithothermal units were constructed by a geostatistical approximation method known as kriging (Davis, 1986; de Marsily, 1986; Willett, 1990).

Kriging was used because each predicted datum is a function of all of the observed data. Moreover, the method provides uncertainties associated with predicted data. Statistical information from a semivariogram is used to find an optimal set of weights that are used in the estimation of values at unsampled locations (Davis, 1986). The uncertainty associated with an estimate is also a function of geographic arrangement, specifically the proximity of the unsampled location to observed data. McPherson (1992) details the algorithm employed in this study.

Thermal conductivity

Thermal conductivities for Powder River Basin rock samples were measured, and appropriate corrections for in-situ conditions were applied (Chapman et al., 1984). Conductivity values were used principally to estimate values of heat flow within the basin. Additionally, the measured values and their variances were used to constrain initial estimates of formation temperature gradient distributions for the stochastic thermal analysis.

In general, thermal conductivity information for all formation from many wells throughout the basin is required for an accurate heat-flow assessment. For this study, however, thermal conductivity data are sparse and unevenly distributed

laterally and vertically. Drill cuttings from the Government Davis no. 5 well, shown on Figure 4, were sampled. Conductivity measurements were made on samples from 95 depth intervals (each 20 ft). The value of conductivity measured in each interval is an average value because cuttings are mixed over the interval.

Thermal conductivities of cuttings were measured using a divided bar apparatus (Roy et al., 1968; Chapman, 1976) and the cell method of Sass et al. (1971). The measured values of matrix thermal conductivity of the rock fragments (k_m) were corrected for in-situ porosity and temperature conditions to produce an estimate of in-situ conductivity ($k_{\text{in situ}}$). Sampling of lithothermal units 5, 6, and 7 was sparse, so thermal conductivities for these units were augmented by published values of matrix thermal conductivity from Decker et al. (1980). Thermal conductivity values used in this study are summarized in Table 1.

TEMPERATURE FIELD

Two different models were used to estimate temperatures within the transect, one by Willett and Chapman (1987a) and the other by Speece et al. (1985). Both are based on a layered-earth model (Bullard, 1947) and the assumption of steady-state, 1-D conductive heat transfer. Also common to both models for this study is that the seven lithothermal units serve as discrete layers. The distinction between the two models lies in assumptions regarding the variability of temperature gradients. For the model of Willett and Chapman (1987a), it is assumed that temperature gradients vary both in position and with depth. Gradients vary laterally within the same unit by specified correlation functions. Furthermore, it is assumed that lateral changes in temperature and temperature gradient are smooth compared to vertical changes (Willett and Chapman, 1987a). This model is therefore referred to as the "laterally variable gradient model." For the model of Speece et al. (1985), temperature gradients are assumed to vary between layers, but to be constant within the same layer. This model is referred to as the "laterally constant gradient model."

Implicit in both layered-earth models is the assumption that temperature at any point in a well may be expressed as the surface ground temperature plus the sum of the temperature changes across each layer between the surface and the point of interest:

$$T(x, y, z) = T_0(x, y) + \sum_{i=1}^{L} z_i g_i, \tag{4}$$

where $T_0(x, y)$ is the surface ground temperature, z_i is the thickness of the ith layer, g_i is the temperature gradient in the ith layer, and the sum is performed $i = 1$ to L over the L layers between the surface and the temperature measurement position. Equation (4), which describes temperature at any point in a well, can also be written

$$(T(x, y, z) - T_0) = \sum_{i=1}^{L} z_i g_i. \tag{5}$$

For N wells a linear system of N equations results, which is expressed in matrix form as

$$\mathbf{d} = \mathbf{G}\mathbf{m}, \tag{6}$$

where $\mathbf{m}$ is the vector of unknown gradients to be solved, $\mathbf{G}$ is the $N \times L$ matrix of unit thicknesses, and $\mathbf{d}$ is the vector of known temperature drops for each well. To find the temperature field, the unknown temperature gradients ($\mathbf{m}$) must first be determined using a linear inversion technique. Equation (4) is then applied to find the temperature at desired depths within each well.

Parameterizations of the two models are different. For the laterally variable gradient model, the number of unknown gradients is $M = N \times L$, where N is the number of observed BHTs and L is the number of layers in the model. The linear inverse problem is underdetermined because $M > N$. For the laterally constant gradient model, the number of unknown temperature gradients is $M = L$. Thus, the linear inverse problem for this model is overdetermined when the number of wells exceeds the number of layers.

Different inversion techniques are required for the two models because of differing parameterization. An L_1 norm inversion technique was used to solve the overdetermined inverse problem of the laterally constant gradient model. Both the Simplex algorithm, discussed in Menke (1984) and applied in Deming and Chapman (1988b), and a reweighted least-squares (RWLS) algorithm were used to find the L_1 norm inverse solution. The concept for the RWLS technique was acquired from Claerbout and Muir (1973); the algorithm was developed for this study and is discussed in McPherson (1992). The stochastic inversion method of Willett (1990) was used for the inverse problem of the laterally variable gradient model. Stochastic inversion is an appropriate technique to apply because the model is very underdetermined and because of the spatial variability of thermal properties.

Table 1. Summary of average matrix thermal conductivities used in thermal analysis. Values for lithothermal units 1 through 4 were measured of samples from the Government Davis no. 5 well (Figure 4). Values for lithothermal units 5 through 7 are from Decker et al. (1980) (EBET 9[a] well).

Lithothermal unit	Number of samples	Depth interval (m)	Mean conductivity (W/m/K)	Standard deviation (W/m/K)
(1) Wasatch-Lance	30	150–1625	3.0	0.8
(2) Fox Hills	20	1625–1811	3.6	0.3
(3) Pierre-Steele	27	2371–2720	2.2	0.5
(4) Niobrara-Belle Fourche	18	2722–2880	2.7	0.5
(5) Mowry-Dakota	11	802–1102	2.2	0.2
(6) Spearfish-Chugwater	19	1432–1602	3.0	0.1
(7) Minnelusa-Tensleep	10	1642–1672	4.4	0.3

Laterally constant gradient model using the Simplex L_1 norm inversion method

The laterally constant gradient model was first applied to the entire transect, and average thermal gradients for the seven lithothermal units were determined. A predicted temperature field was then constructed at each well using equation (4) and the estimated gradients. A temperature residual [difference between observed (corrected) BHT and BHT predicted by the model] was calculated at each BHT measurement position. The mean residual for this first application of a laterally constant gradient model was 8°C (Figure 6). This residual is considerably less than the mean residual obtained by assuming a uniform gradient model (a single gradient for all strata within the entire region). For example, if one applies

$$T(z) = T_0 + g_{\text{mean}} z \tag{7}$$

to all wells, where g_{mean} is the average thermal gradient (29°C/km) for all lithothermal units, the mean residual for the temperature field is around 18°C.

Resolution for the laterally constant gradient model can be improved by subdividing the transect into smaller region and analyzing each separately. We arbitrarily subdivided the transect into six regions of equal size and then applied the laterally constant gradient model in each region. The mean value of absolute residual for all 1807 wells decreased from 8°C to 5.5°C with this regionalization. Further subdivision into 9 and 18 equal regions improved resolution only slightly more, as shown in Figure 6, but solution stability decreased with subdivision.

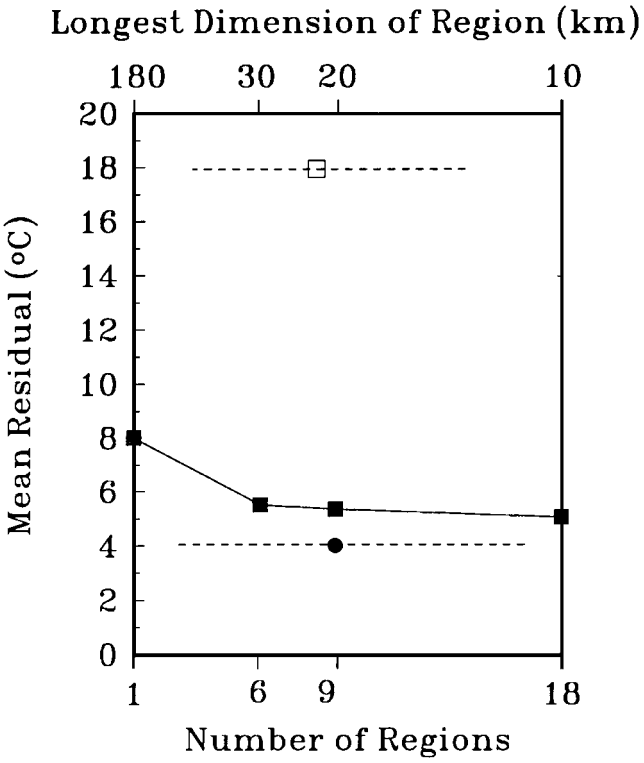

FIG. 6. Comparison of goodness-of-fit for 6, 9, and 18 equal-sized regions for the laterally constant gradient model. The mean residual for the laterally constant gradient model (for which no regionalization was required) is shown (solid circle), as well as the mean residual for temperatures calculated assuming a uniform regional thermal gradient (29°C km^{-1}) for all strata (open box).

The six-region model seemed to be a sufficient compromise of the tradeoff between solution stability and resolution. Table 2 reports the calculated temperature gradients (G) for lithothermal units 1 through 7, by region, for only those data within each region. Excepting null values, temperature gradients range from 2.7°C/km up to almost 220°C/km. Temperature gradients for both units 2 (Fox Hills) and 7 (Minnelusa-Tensleep) show considerable fluctuation from region to region. More specifically, in four of the regions unit 2 exhibits the highest gradient. This tendency is counterintuitive because unit 2 has a relatively high matrix thermal conductivity (3.6 W/m/K), and temperature gradients are inversely proportional to conductivity (Fourier's law of heat conduction). These two units, however, each represent less than 2 percent of the entire sedimentary section (Table 2), and previous studies (Speece et al., 1985; Deming and Chapman, 1988a) determined that temperature gradients of units that are relatively underrepresented tend to have large standard deviations. These studies also concluded that in spite of the large uncertainty associated with these gradients, the estimated temperature field was not significantly affected. Null values of estimated gradient are assumed to be an artifact of the inversion; the two null gradients estimated for region 6 are for units 2 and 7, the relatively underrepresented units.

For the five lithothermal units representing individually more than 5 percent of the stratigraphic section (Table 2), some systematic variations in temperature gradient are evident. For example, unit 3 (Pierre-Steele), which has the lowest value of matrix thermal conductivity (Table 1), shows relatively high gradients within regions 1, 2, 4, and 5. However, unit 5 (Mowry-Dakota), which shares the same lowest value of matrix conductivity, shows relatively high gradients only in region 1. Thus we attach only marginal significance to much of the variation of the temperature gradients reported in Table 2.

The temperature field for cross-section A–A′ estimated using the gradients calculated for the laterally constant gradient model (six regions) using the Simplex L_1 norm inversion technique is shown in Figure 7. A discrete temperature field was calculated for each of the six regions, with the lateral variability within each depending directly on the variability of unit thicknesses. Isotherms at the borders of the six regions were slightly discordant. However, constraining temperatures

Table 2. Preferred temperature gradients calculated for the laterally constant gradient model. Γ_1 through Γ_7 are temperature gradients in °C/km for lithothermal units 1 through 7, respectively, listed by region. Listed at the bottom of the table is the relative proportion of each unit with respect to the sedimentary section within the transect, penetrated by wells.

Region	Γ_1	Γ_2	Γ_3	Γ_4	Γ_5	Γ_6	Γ_7
1	66.3	219.3	41.5	22.2	55.5	21.9	25.9
2	14.8	36.9	42.1	10.3	12.9	36.1	25.9
3	21.8	4.1	29.8	40.2	8.9	19.1	2.7
4	19.8	47.7	38.8	25.3	30.1	16.2	24.1
5	24.4	44.6	32.3	24.5	29.1	36.3	21.1
6	37.1	0.0	22.8	21.6	26.2	16.7	0.0
Proportion (%)	41.8	1.9	30.6	11.9	7.0	5.4	1.4

to match between region borders in the inversion was not necessary and isotherms between region borders were matched by smoothing.

Predicted temperatures on the cross-section vary from 9°C at the surface up to 120°C at 4.5 km depth. Compressed isotherms beneath the eastern limb of the Salt Creek Anticline (distance 20 km northeast of A on profile A–A′) are consistent with the high average temperature gradients of the area. Just east of the anticline and coincident with the basin axis, isotherms become more depressed. East of the basin axis, temperatures generally increase with dip, but closest to A′ isotherms are again depressed.

Laterally variable temperature gradient model using the stochastic inversion method

Using corrected BHTs as the primary data, Powder River Basin lithothermal unit temperature gradients were estimated by stochastic inversion. The average lithothermal unit temperature gradient determined by the laterally variable gradient model and stochastic inversion is 29°C/km, consistent with the mean temperature gradient for the composite temperature-versus-depth plot. Lithothermal unit temperature gradients among all seven units vary from 8°C/km to 78°C/km. Unit 1 gradients vary the most along the transect, whereas unit 7 (Minnelusa-Tensleep) varies the least.

A temperature field for cross-section A–A′ constructed from stochastic inversion gradient results is shown in Figure 8. Predicted temperatures within the sedimentary section on the cross-section vary from 9°C at the surface to almost 130°C at 5 km depth. The temperature field for A–A′ using the laterally constant gradient model (Figure 7) is qualitatively similar; isotherms beneath the eastern limb of the Salt Creek Anticline are compressed, a general increase of temperature occurs between the basin axis and 160 mm from A, and east of 160 km isotherms are deeper and less compressed, indicative of lower temperature gradients. The temperature field of Figure 8 (laterally variable gradient model) shows more detail than that of Figure 7 (laterally constant gradient model) because data resolution is higher, a consequence of more degrees of freedom in the model parameterization. An expression of this improved fit of the temperature field is a mean residual of 4.0°C (Figure 6), constituting a 29 percent residual reduction compared to that of the six-region laterally constant gradient model.

Also shown in Figure 8(b) is the level of variance associated with the estimated temperature field. Values of variance range from 2 $(°C)^2$ to 8 $(°C)^2$. Error is lowest in the vicinity of observed data, at the surface and the depths of BHT measurements. The position of each BHT measurement is plotted on the cross-section to illustrate that associated errors surrounding BHT measurement depths are relatively low.

Discussion of models and geophysical inversion methods

The laterally variable gradient model in conjunction with the stochastic inversion method provided better resolution than the laterally constant gradient model. An overlay of histograms of temperature residual corresponding to the two models is shown in Figure 9. Over 1250 of the residual calculated by the former were between −5°C and 5°C; just over 1000 calculated by the latter model were in the same range. The distributions have very similar shapes (Figure 9), but the distribution for the laterally variable gradient model is more peaked (light-tailed) than the distribution of the laterally constant gradient model. The mean of the absolute values of residuals for the laterally variable gradient model is 4°C; for the laterally constant gradient model, the mean is 5.6°C for the six-region case and 8°C for the single-region case (See Figure 6).

In general, for areas less than a few square kilometers, the solutions and temperature fields obtained from different models converge. To demonstrate this, a 1 km^2 area with high well density (15 wells) was analyzed using both models. The resulting temperature fields, estimated accuracy, and data resolution by both inversion methods were approximately the same. It is thus concluded that either of these models may be used for areas less than a few square kilometers, provided sufficient well data are available.

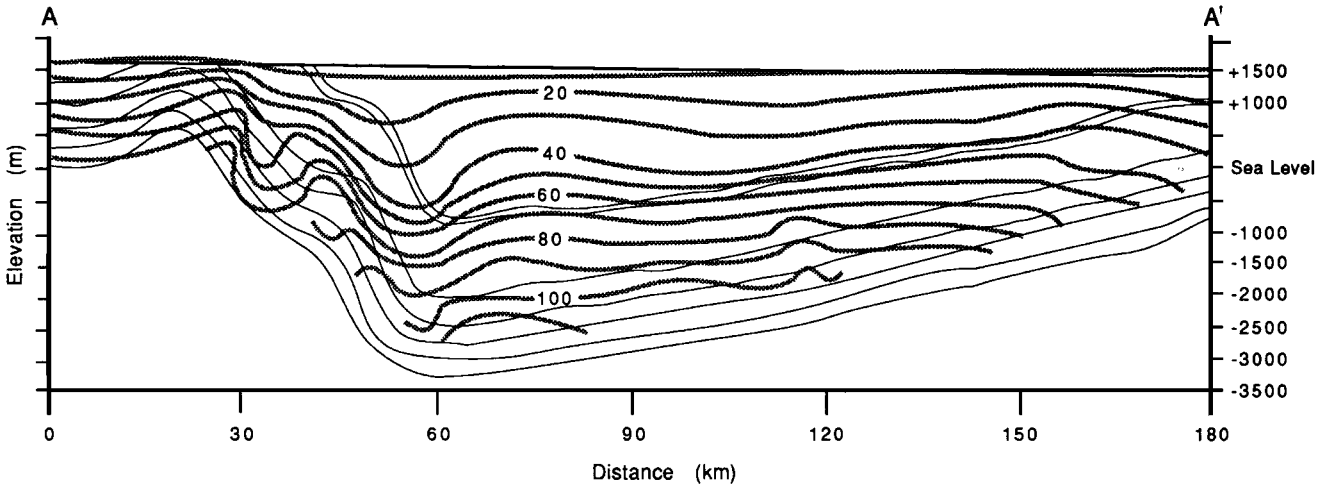

FIG. 7. Two-dimensional temperature field for cross-section A–A′ calculated from the laterally constant gradient model in conjunction with L_1 norm inversion. The temperature field in each of six equal regions (regionalization discussed in text) is calculated by combining thermal gradients from Table 2 and local structure of lithothermal units and smoothing at region boundaries. Contour label is °C.

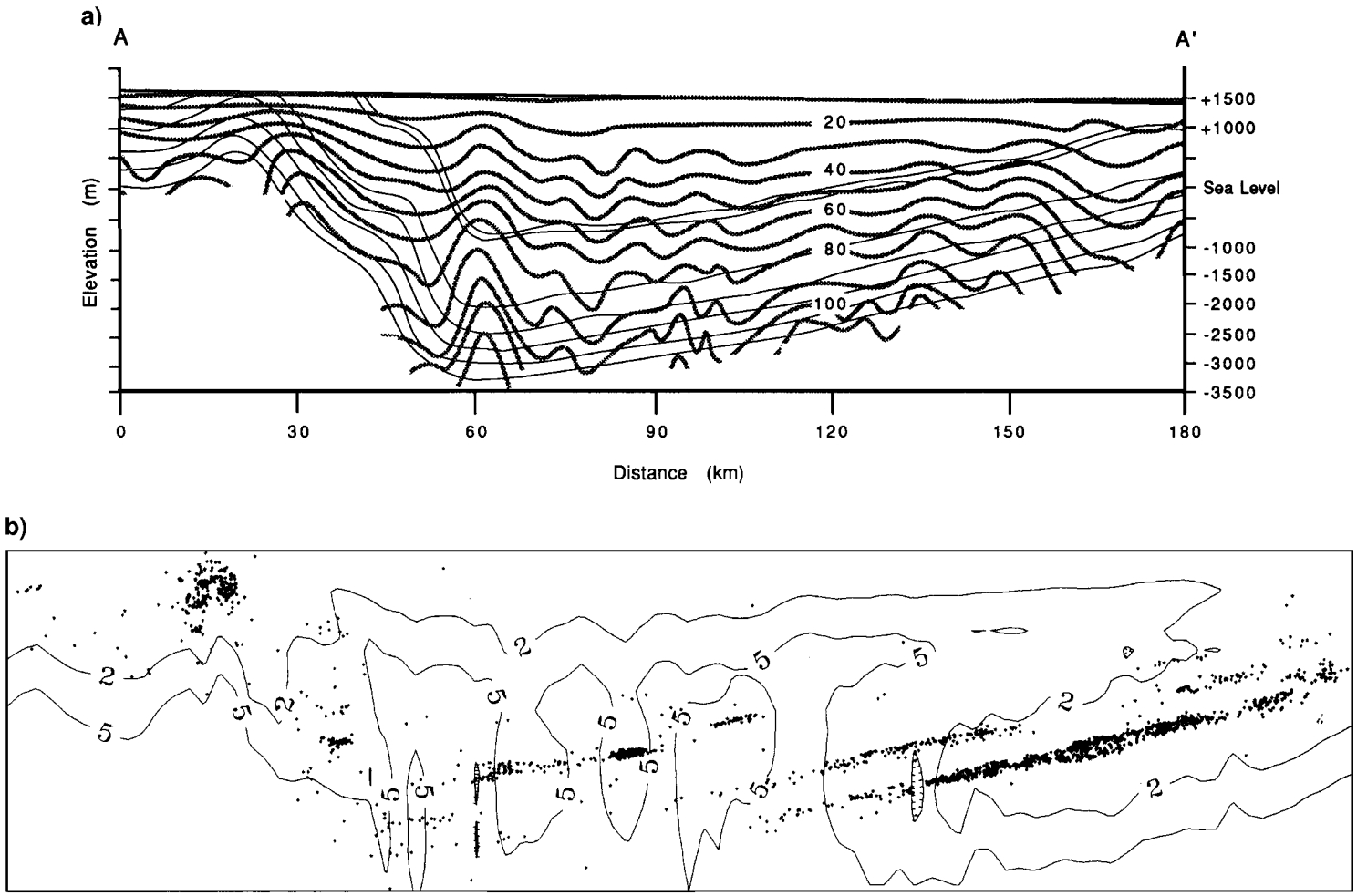

FIG. 8. (a) Two-dimensional temperature field and (b) associated variances for cross-section A–A′ calculated using the laterally variable gradient model and stochastic inversion. The temperature contour interval for the temperature field (top) is 10°C and the variance contour interval for the map of variances (bottom) is $3°C^2$. The depths of the 1807 BHT measurements are projected onto the bottom cross-section, illustrating that high values of estimated variance are associated with low data density.

If the study area is sufficiently small and if computational convenience is a concern, the overdetermined problem is easy to model using the RWLS or Simplex techniques. The RWLS inversion algorithm is simplest conceptually, and the computer code is relatively easy to construct with available matrix algebra libraries. The Simplex algorithm is well known and several computer codes have been published. However, for large study areas, subdividing the area into discrete regions for individual analysis is necessary for the overdetermined cases. This is inconvenient because determining the optimum distribution of regions must be done by trial and error. Additionally, estimating statistical accuracy for the L_1 norm solution is difficult. For the general case, regardless of study area size, solving the underdetermined problem using the variable gradient model with the stochastic inversion technique obviates the other methods.

HEAT FLOW IN THE SOUTHERN POWDER RIVER BASIN

Heat flow q is calculated using Fourier's law of heat conduction

$$q = -k\nabla T, \tag{8}$$

where k is thermal conductivity, and ∇T is the thermal gradient across the rock unit(s) of interest. For the Powder River Basin transect, one-dimensional conductive heat transfer was assumed. Surface heat flow q_i at the ith well (of the 1807) was estimated using a modified form of equation (8),

$$(\mathrm{BHT} - T_{\mathrm{surface}})_i = q_i \left(\sum_{j=1}^{L} z_j/k_j \right), \qquad j = 1 \text{ to } L, \tag{9}$$

where z_i is the rock unit thickness, k_j is the thermal conductivity of the jth lithothermal unit corrected for in-situ conditions, and the sum is performed over the L layers between the surface and the BHT depth. The quotient z_j/k_j is referred to as thermal resistance.

The distribution of surface heat flow across profile A–A′ of the Powder River basin transect, calculated with equation (9), is shown in Figure 10. With two local exceptions, heat flow generally varies between 40 mW/m^2 and 60 mW/m^2 with an average value of 52 mW/m^2. The most general feature of the distribution is the gradual eastward increase of heat flow between profile distances 40 km and 150 km from A, reflecting the general structure of the basin. Beyond this first-order heat flow pattern, two exceptional features were observed: high heat flow values in the vicinity of the Salt Creek Anticline and Teapot Dome (both ~15 km northeast of A) and an abrupt decrease in heat flow occurring between profile distances 150 km and 180 km.

Previous heat-flow measurements in the western periphery of the Black Hills (Decker et al., 1980; Backwell, 1969; Sass et al., 1971) range from 21 to 88 mW/m^2 whereas heat-flow values assessed in this study in the northeastern part of our transect range only between 40 and 52 mW/m^2. Blackwell (1969)

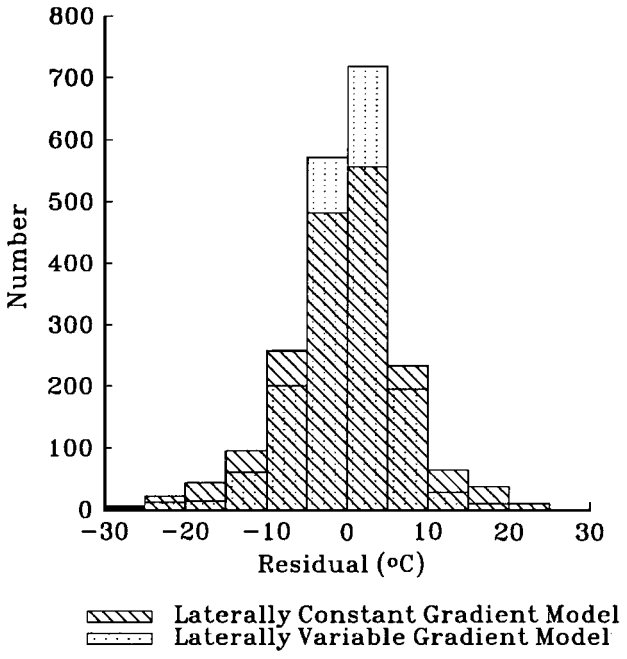

FIG. 9. Overlay of histograms of temperature residuals corresponding to two temperature models. The mean of the absolute values of residuals for the laterally variable gradient model is 4.0°C; for the laterally constant gradient model (six-region case), the mean is 5.0°C.

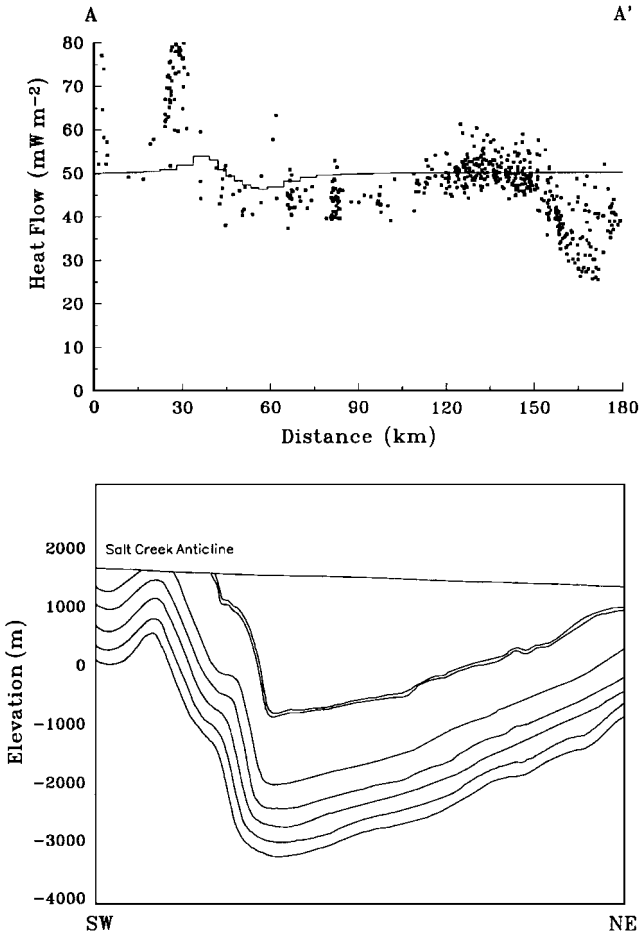

FIG. 10. Surface heat flow versus distance along profile A–A′ superimposed over cross-section A–A′. The solid line indicates finite-element model results.

estimated two heat-flow values adjacent to the Black Hills and within the Powder River Basin. One of these estimates is located in the study area of this report (Figure 1) and has a value of 75 mW/m^2, within 2 mW/m^2 of the value calculated for the same location in this study.

Discussion of heat-flow regime

Three prominent features of the surface heat-flow regime are also common to the average gradient distribution and the preferred temperature field (see Figure 10): (1) the general asymmetric heat-flow pattern similar to the structure of the basin (higher over the limbs and lower over the axis), (2) the high heat flow associated with the Salt Creek anticline and the Teapot Dome, and (3) the heat-flow depression at the northeast end of the transect collocated with the confluence of the Belle Fourche River, Buffalo Creek, Raven Creek, Timber Creek, and several other smaller tributaries (Figure 1).

Anomalies (2) and (3) are considered to be of hydrologic origin, although numerical modeling is necessary to verify this explanation. The local heat-flow high associated with the Salt Creek anticline is interpreted using local and regional information. Several units crop out in this area, including the Niobrara-Belle Fourche unit, a the apex of the anticline. Love and Christiansen (1985) indicate many small faults in the vicinity of, and possibly attributed to, this anticline that may increase the local permeability. Given that the anticline trends almost due north and plunges toward the south, the Laramie Mountains to the southwest are possibly a source of topographically driven fluids which are channeled through one or more of the local sedimentary units and discharged at this locality. Thus, the elevated temperatures could be attributed to advective heat flow associated with local discharge of water heated at depth.

The distinct thermal depression which occurs in the northwest end of the transect can also possibly be explained by an advective disturbance. Recharge of surface water from the local drainage system (the confluence of rivers and creeks within the study area shown in Figure 1) may have a cooling effect. However, decreased temperatures extend to depths of 3.5 km and would require recharge rates likely in excess of what actually occurs from this river system. A more likely explanation involves deep groundwater flow along the Minnelusa-Tensleep (unit 7). Detailed hydrologic information and/or numerical simulations would be useful to elucidate possible causes of these thermal anomalies.

The most general heat-flow pattern which mimics basin structure has several possible explanations. First, if a uniform basal heat flux for the region and one-dimensional, steady-state conductive heat transfer are assumed, variations of the thermal conductivity distribution [$k = k(z)$ or $k = k(x, z)$] govern the first-order temperature pattern (assuming insignificant radiogenic heat production). However, holding basal heat flow constant, surface heat flow $q(x, y)$ over the transect would be constant as well (one-dimensional heat flow). The pattern of observed surface heat flow for the transect is not uniform but is very similar to that of average gradients, thus precluding this explanation under these assumptions.

Second, assuming two-dimensional, steady-state conductive heat flow and a uniform [$q = q(x) =$ constant] basal heat flux, the pattern may be interpreted as a consequence of heat-flow refraction, given that the conductivity of the sediments is lower than that of the basement strata (Decker et al., 1980). This hypothesis was tested by modeling the basin using a two-dimensional finite-element method (Forster and Smith, 1988). The algorithm models the steady-state conductive temperature field and surface heat flow accounting for the effects of a variable thermal conductivity structure and specified boundary conditions. A finite-element mesh was constructed, patterned after cross-section A–A′ (Figure 2). The seven lithothermal units were collectively one unit assigned a thermal conductivity value of 1.7 W/m/K, the average value of in-situ conductivity for the seven units within the transect. Basement strata down to 10 km depth were assigned a thermal conductivity of 3.7 W/m/K, the conductivity of nearby Jeffrey City Precambrian granites measured by Decker et al. (1980). Boundary conditions in the model include constant, uniform basal heat flow of 50 m/W/m^2. Figure 10 shows the surface heat-flow profile for cross-section A–A′ estimated by the model. The modeled profile also mimics the basin structure, albeit to a lesser extent. Highest predicted values occur just west of the Salt Creek Anticline, consistent with observed values and probably caused by the focusing of refracted heat through basement strata along the steep dipping west limb of the basin syncline. Predicted heat flow is lowest at the basin axis, and increases to the basal heat flow value (50 mW/m^2) eastward. The lack of a significant increase of heat flow on the eastern side of the basin is likely due to the dip of this side of the basin syncline being much less than the western limb; refracted heat is less focused on this side. Further refinement of the thermal conductivity structure in the mesh and/or adjusting the value of basal heat flow could permit a better match between the observed data and the modeled profile. However, the simple model was run only to test the quantitative effect of heat refraction due to thermal conductivity contrast.

Third, under a transient, one-dimensional conductive heat-flow assumption, sedimentation within the center of the basin could be decreasing heat flow close to the basin axis while erosion at the flanks increases heat flow around the periphery. This hypothesis was tested by numerically modeling the burial and uplift history of the basin while tracking surface heat flow with time. A finite-difference method (Deming and Chapman, and Chapman 1988b) was used to model the surface heat-flow history at three wells within the transect including a well at A, one at A′, and one at the basin axis on profile A–A′. Details of the geologic history of the basin used in simulations were taken from Thomas (1949), Tenney (1966), High and Picard (1969), and Hagmaier (1971), and are summarized in McPherson (1992). Radiogenic heat production was not considered, and basal heat flow was held constant throughout basin history at 50 mW/m^2.

At the basin axis well, present day surface heat flow was reduced by 2 mW/m^2 (4%) relative to the input basal heat flow. Conversely, at both periphery wells, present day surface heat flow was increased by 4 mW/m^2 (8%) relative to basal heat flow. These results demonstrate that the effects on surface heat flow by sediment deposition and erosion, although relatively minor, are complementary to the refraction effects caused by heterogeneous thermal conductivity structure.

A variable surface heat flux could also be caused by laterally variable basement heat production. Decker et al. (1980)

report a value of 5 $\mu W/m^3$ for heat production of Precambrian granite at Jeffrey City. A change in basement heat production of 1 $\mu W/m^3$ to a depth of 5 km would cause a change in heat flow by 5 mW/m^2 and such changes are quite possible along a 180 km profile, although difficult to detect. Sedimentary heat production is characteristically 1 $\mu W/m^3$ and is likely not the cause of lateral heat-flow variations in the Powder River Basin.

Finally, assuming transient, three-dimensional conductive heat flow, all or any combination of the above processes could be occurring simultaneously. This is assumed to be the case, although heat-flow refraction due to the contrast in thermal conductivity between basement strata and sediments is probably the greatest factor affecting the first-order thermal pattern.

CONCLUSIONS

Analysis of temperatures and geologic data from over 1800 oil and gas wells within a 180 km by 30 km transect in the Powder River Basin lead to the following conclusions:

1) Temperature fields for the Powder River Basin transect were computed for models of varying complexity. The mean residual temperature between the observed (corrected) BHT and the model temperature is a measure of the model suitability: (a) A uniform gradient model for the entire basin produced an average gradient of 29°C/km, but also produced a high mean residual of ~18°C. (b) A laterally constant gradient model in conjunction with Simplex L_1 norm inversion yielded a mean residual of 8°C, which was further reduced to 5.5°C by dividing the transect into six equal-sized regions. (c) A laterally variable gradient model in conjunction with stochastic inversion produced the best fitting temperature field with a mean residual of 4°C, close to the corrected BHT error.
2) Matrix thermal conductivities were measured for 95 samples from the Government Davis no. 5 well near the center of the transect. Values of rock matrix conductivity at 20°C vary between 1.9 W/m/K and 4.6 W/m/K. Thermal conductivity at in-situ conditions was computed by making appropriate corrections for porosity, pore-fluid conductivity and temperature.
3) The preferred temperature field in conjunction with measured thermal conductivities were used to calculate surface heat flow within the transect. The average heat flow for the southern Powder River Basin, calculated from 1807 observed values within the transect studied, is 52 mW/m^2. Except in three local areas, surface heat flow varies between 40 mW/m^2 and 60 mW/m^2 along the transect, with a pattern very similar in shape to the basin structure. This first-order thermal pattern is interpreted to be due primarily to refraction of heat flow through basement strata which have higher thermal conductivity than the sedimentary section, but may also be influenced by sedimentation (deposition) that reduces heat flow at the basin axis and erosion that enhances surface heat flow at the basin periphery. Extremely high heat flow in the region occurs in two areas. Values up to 225 mW/m^2 are observed at the Teapot dome, and up to 150 mW/m^2 values are observed at the Salt Creek anticline. Low heat flow down to as low as 25 mW/m^2 occurs locally near the northeast end of the transect. All three of these anomalies are likely caused by groundwater movement. Heat flow within the southern Powder River Basin transect determined from the analysis of petroleum well data is consistent with and forms a useful complement to heat flow measured by more standard techniques in other parts of Wyoming.

ACKNOWLEDGMENTS

Acknowledgment is made to the donors of the Petroleum Research Fund, administered by the ACS, for support of this research under grant no. 20170-AC2-C.

REFERENCES

Bauer, M. S., and Chapman, D. S., 1986, Thermal regime at the Upper Stillwater dam site, Uinta Mountains, Utah: Implications for terrain, microclimate and structural corrections in heat flow studies: Tectonophysics, **128**, 1–20.
Beck, A. E., and Shen, P. Y., 1985, Temperature distribution in flowing liquid wells: Geophysics, **50**, 1113–1118.
Blackwell, D. D., 1969, Heat flow determinations in the northwestern United States: J. Geophys. Res., **74**, 993–1007.
Bullard, E. C., 1947, The time necessary for a borehole to attain temperature equilibrium: Mon. Not. Roy. Astr. Soc., **5**, 127–130.
Cao, S., Lerche, I., and Hermanrud, C., 1988, Formation temperature estimation by inversion of borehole measurements: Geophysics, **53**, 979–988.
Carvalho, H. D. S., and Vacquier, V., 1977, Method for determining terrestrial heat flow in oil fields: Geophysics, **42**, 584–593.
Chapman, D. S., 1976, Heat flow and heat production in Zambia: Ph.D. thesis, Univ. of Michigan.
Chapman, D. S., Keho, T. H., Bauer, M. S., and Picard, M. D., 1984, Heat flow in the Uinta Basin determined from bottom hole temperature (BHT) data: Geophysics, **49**, 453–466.
Claerbout, J. F., and Muir, F., 1973, Robust modeling with erratic data: Geophysics, **38**, 826–844.
Davis, J. C., 1986, Statistics and Data Analysis in Geology: Wiley & Sons.
Decker, E. R., Baker, K. R., Bucher, G. J., and Heasler, H. P., 1980, Preliminary heat flow and radioactivity studies in Wyoming: J. Geophys. Res., **85**, 311–321.
de Marsily, G., 1986, Quantitative hydrogeology, groundwater hydrology for engineers: Academic Press Inc.
Deming, D., 1989, Application of bottom-hole temperature corrections in geothermal studies: Geothermics, **18**, 775–786.
Deming, D., and Chapman, D. S., 1988a, Heat flow in the Utah-Wyoming thrust belt from analysis of bottom-hole temperature data measured in oil and gas wells: J. Geophys. Res., **93**, 13657–13672.
——— 1988b, Inversion of bottom-hole temperature data: The Pineview field, Utah-Wyoming thrust belt: Geophysics, **53**, 707–720.
Forster, C. B., and Smith, L., 1988, Groundwater flow systems in mountainous terrain, 1. Numerical modeling technique: Water Resources Research, **24**, 999–1010.
Hagmaier, J. L., 1971, Groundwater flow, hydrochemistry, and uranium deposition in the Powder River basin: Wyoming, Ph.D. thesis, Univ. of North Dakota.
High, L. R., and Picard, M. D., 1969, Stratigraphic relations within Upper Chugwater Group (Triassic), western Wyoming: Mountain Geologist, **4**, 73–81.
Horner, D. R., 1951, Pressure build-up in wells: Proc. Third World Petroleum Congress, The Hague.
Jaegar, J. C., 1965, Application of the theory of heat conduction to geothermal measurements, *in* Lee, W.H.K., Ed., Terrestrial heat flow: Am. Geophys. Union, Geophys. Monographs 8, 7–23.
Jones, F. W., Rahman, M., and Leblanc, Y., 1984, A three-dimensional numerical bottom-hole temperature stabilization model: Geophys. Prosp., **32**, 18–36.
Lee, T., 1982, Estimation of formation temperature and thermal property from dissipation of heat generated by drilling: Geophysics, **47**, 1577–1584.
Love, J. D., and Christiansen, A. C., 1985, Geologic map of Wyoming: U.S. Geol. Survey, Reston, Va.
Luheshi, M. N., 1983, Estimation of formation temperatures from borehole measurements: Geophys. J. Roy. Astr., Soc., **74**, 747–776.
Majorowicz, J. A., and Jessop, A. M., 1981, Regional heat flow patterns in the western Canadian sedimentary basin: Tectonophysics, **74**, 209–238.
McPherson, B. J. O. L., 1992, Geothermal analysis of the southern Powder River Basin, Wyoming: M.S. thesis, Univ. of Utah.

Menke, W., 1984, Geophysical data analysis: Discrete inverse theory: Academic Press Inc.
National Oceanic and Atmospheric Administration, 1989, Wyoming climatological data: Volume 98, No. 1.
Powell, W. G., Chapman, D. S., Balling, N., and Beck, A.E., 1988, Continental heat flow density *in* Haenel, R., Rybach, L., and Stegena, L., Eds., Handbook of terrestrial heat flow density determination: Kluwer.
Roy, R. F., Decker, E. R., Blackwell, D. D., and Birch, F., 1968, Heat flow in the United States: J. Geophys. Res., **73**, 5207–5221.
Sass, J. H., Lachenbruch, A. N., Munroe, R. S., Green, G. W., and Moses, T. H., Jr., 1971, Heat flow in the Western United States: J. Geophys. Res., **76**, 6376–6413.
Sharp, W. N., and Gibbons, A. B., 1964, Geology and uranium deposits of the southern part of the Powder River Basin, Wyoming: U.S. Geol. Surv. Bull., 1147-D.
Speece, M. A., Bowen, T. D., Folcik, J. L., and Pollack, H. N., 1985, Analysis of temperatures in sedimentary basins: The Michigan Basin: Geophysics, **50**, 1318–1334.
Tenney, C. S., 1966, Pennsylvanian and Lower Permian deposition in Wyoming and adjacent areas: AAPG Bull., **50**, 227–250.
Thomas, H. D., 1949, The geological history and geological structure of Wyoming: Wyo. Geol. Surv. Bull., **42**.
Willett, S. D., and Chapman, D. S., 1987a, On the use of thermal data to resolve and delineate hydrologic flow systems in sedimentary basins; an example from the Uinta Basin, Utah *in* Hitchon, B., Bachu, S., and Sauveplane, C., Eds., Proceedings of the Third annual Canadian/American Conference on Hydrogeology; Hydrology of Sedimentary Basins—Applications to Exploration and Exploration: National Water Well Association.
——— 1987b, Analysis of temperatures and thermal processes in the Uinta Basin, *in* Beaumont, C., and Tankard, A. J., Eds., Sedimentary basins and basin-forming mechanisms: Can. Soc. Petr. Geol. Memoir, **12**, 447–461.
Willett, S. D., 1990, Stochastic inversion of thermal data in a sedimentary basin: Resolving spatial variability: Geophys. J. Int., **103**, 321–339.